Supporting Information

Nylon binder unlocks high-performance flexible thick electrodes prepared in water-based environment

Li Jiang, ‡ [a] *GuoJing Zang,* ‡[a] *Xiu Liu,* [a] *Ling Chen,* [a] *Yaoguang Chen,* [b] *Jinghao Xie,* [a] *Zhongxin Liang,* [c] *Fuzhen Li,* [a] *Zishou Zhang* *[a]

a. Key Laboratory for Polymeric Composite and Functional Materials of Ministry of Education, Key Laboratory of High-Performance Polymer-Based Composites of Guangdong Province, School of Chemistry, Sun Yat-sen University, Guangzhou510275, China. E-mail: zhzish@mail.sysu.edu.cn

b. School of Chemistry and Chemical Engineering, Lingnan Normal University, Guangdong, 524048, China.

c. Department of Physics and Texas Center for Superconductivity at the University of Houston (TcSUH), Houston, TX 77204, USA.

‡ L. J. and G. Z. contributed equally to this work.

Figures:

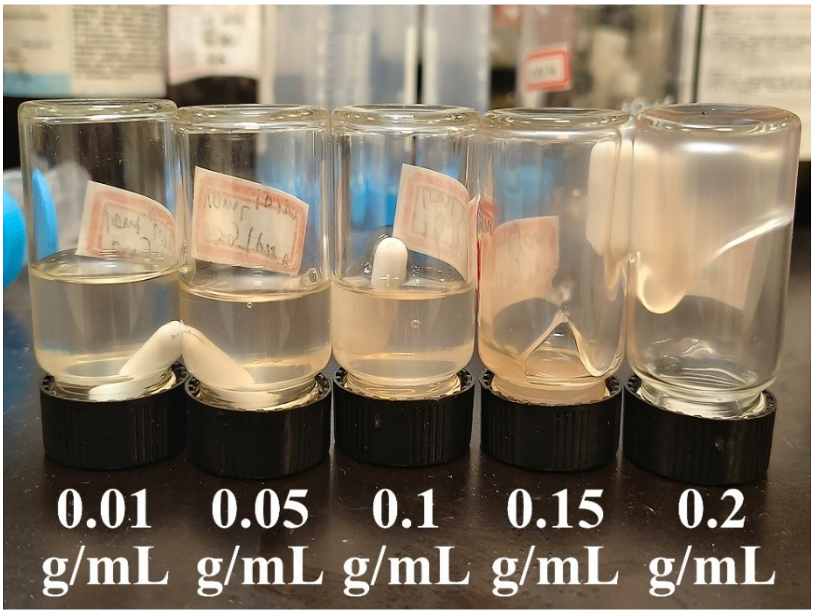

Fig S1. Photos of 0.01-0.2 g·mL^{-1} TPAE/LiTFSI/Water (10 M) solution.

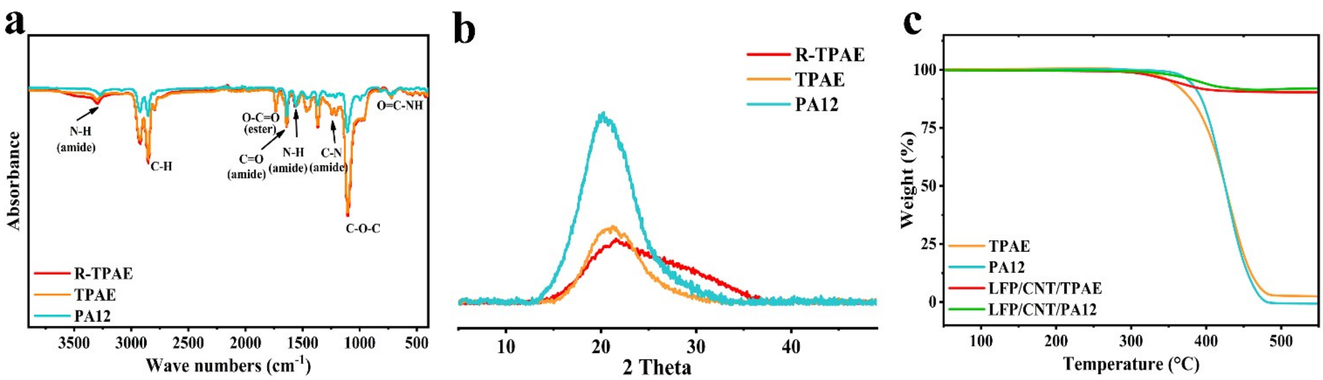

Fig S2. (a) FTIR spectra of TPAE, PA12, and R-TPAE. (b) XRD patterns of TPAE, R-TPAE, and PA12. (c) The TGA plots of TPAE, R-TPAE, PA12, LFP/CNT/TPAE, and LFP/CNT/PA12.

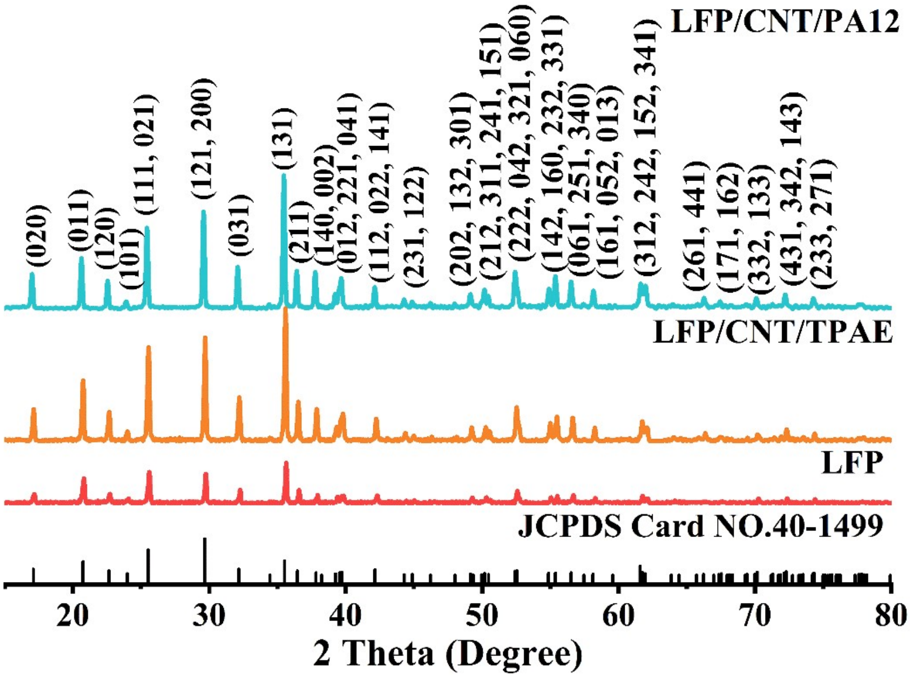

Fig S3. XRD patterns of LFP, LFP/CNT/TPAE, and LFP/CNT/PA12.

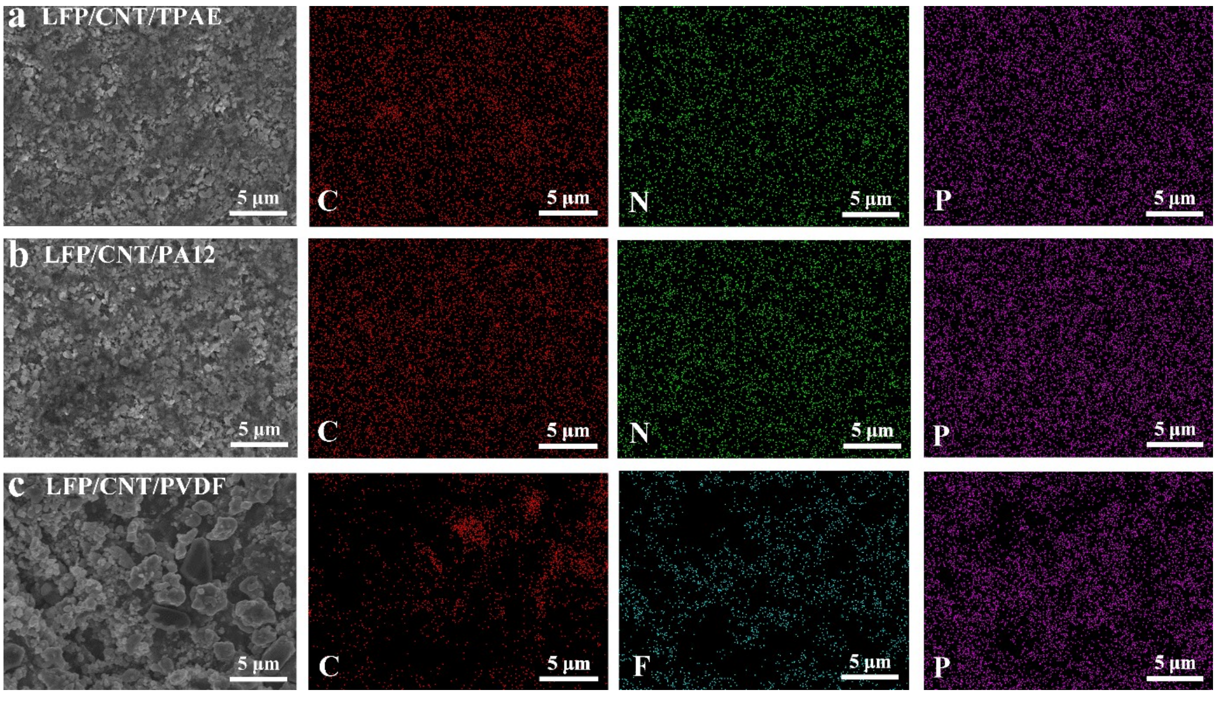

Fig S4. SEM-EDS images of (a) LFP/CNT/TPAE, (b) LFP/CNT/PA12, and (c) LFP/CNT/PVDF.

Table S1. Test results of Mercury porosimetry.

Sample name	Porosity (%)	Average pore diameter (4V/A/nm)	Median pore diameter (V/nm)	Total pore volume (ml·g^{-1})	Total pore area (m^2·g^{-1})
LFP/CNT/TPAE-3 mm	46.0204	108.81	126.64	0.3264	11.999
LFP/CNT/TPAE-200 μm	56.2402	148.65	2,958.36	0.6174	16.615
LFP/CNT/TPAE-100 μm	64.9344	347.83	76,790.13	0.8857	10.185
LFP/CNT/TPAE-20 μm	71.5304	499.22	50,765.03	1.1122	8.911
LFP/CNT/PA12-20 μm	72.8071	403.13	30,388.68	1.1491	11.401

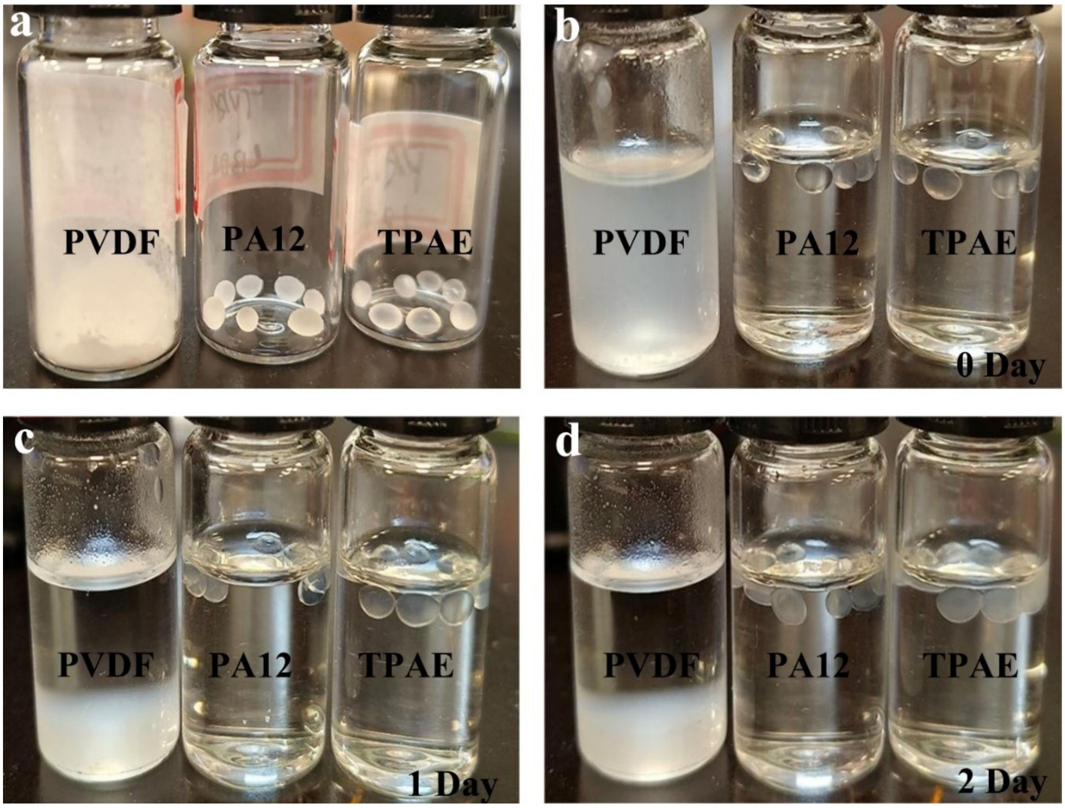

Fig S5. (a) Photos of TPAE particles, PA12 particles, and PVDF powder. Photos of the TPAE 0-day (b), 1-day (c), and 2-day (d) immersion in the electrolyte of 1 M $LiPF_6$ dissolved in EC/DMC/EMC (1:1:1 by volume) at 25°C.

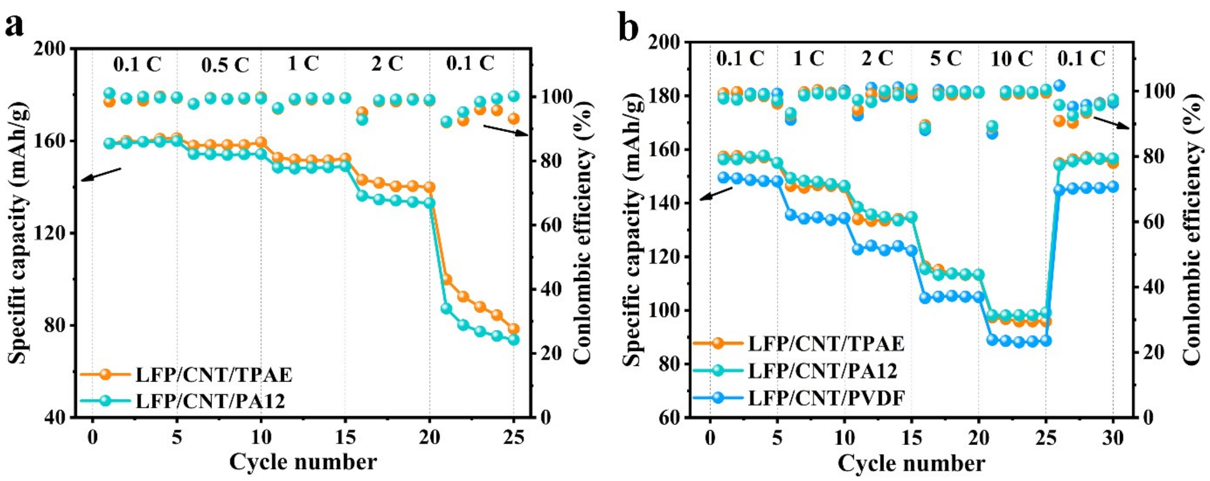

Fig S6. (a) Rate capabilities of LFP/CNT/TPAE and LFP/CNT/PA12 with a mass loading of ~ 30.0 mg·cm^{-2}. (b) Rate capability of LFP/CNT/TPAE, LFP/CNT/PA12, and LFP/CNT/PVDF electrodes with a mass loading of ~ 2.0 mg·cm^{-2} (~ 20 μm).

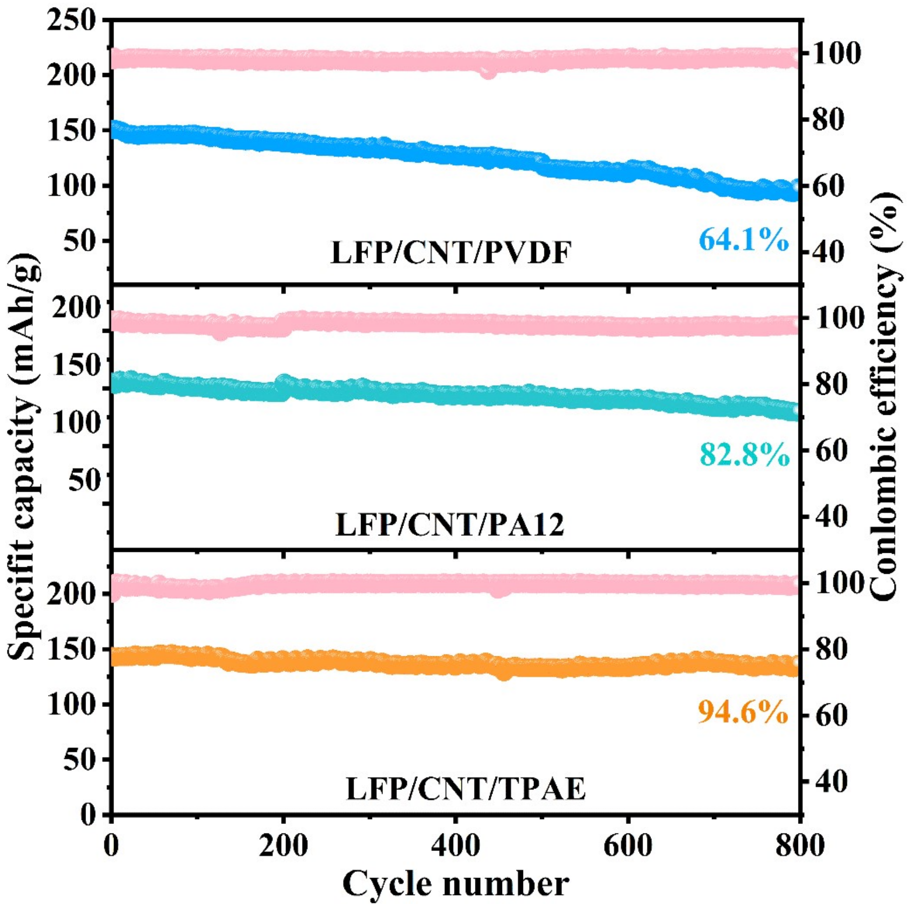

Fig S7. Cycling performance of LFP/CNT/TPAE, LFP/CNT/PA12, and LFP/CNT/PVDF cells with a mass loading of 2.0 mg·cm^{-2} (~ 20 μm) at 1.0 C.

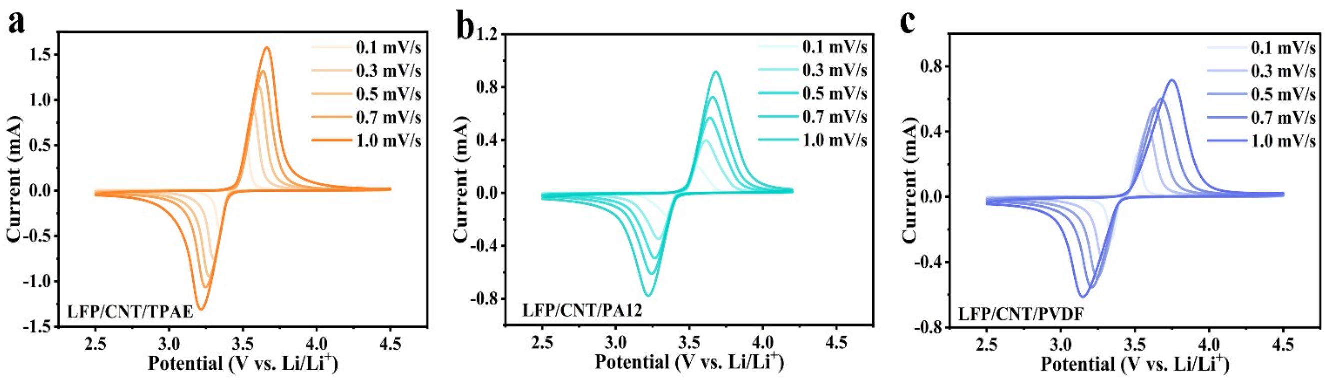

Fig S8. CV curves of (a) LFP/CNT/TPAE, (b) LFP/CNT/PA12, and (c) LFP/CNT/PVDF electrode.

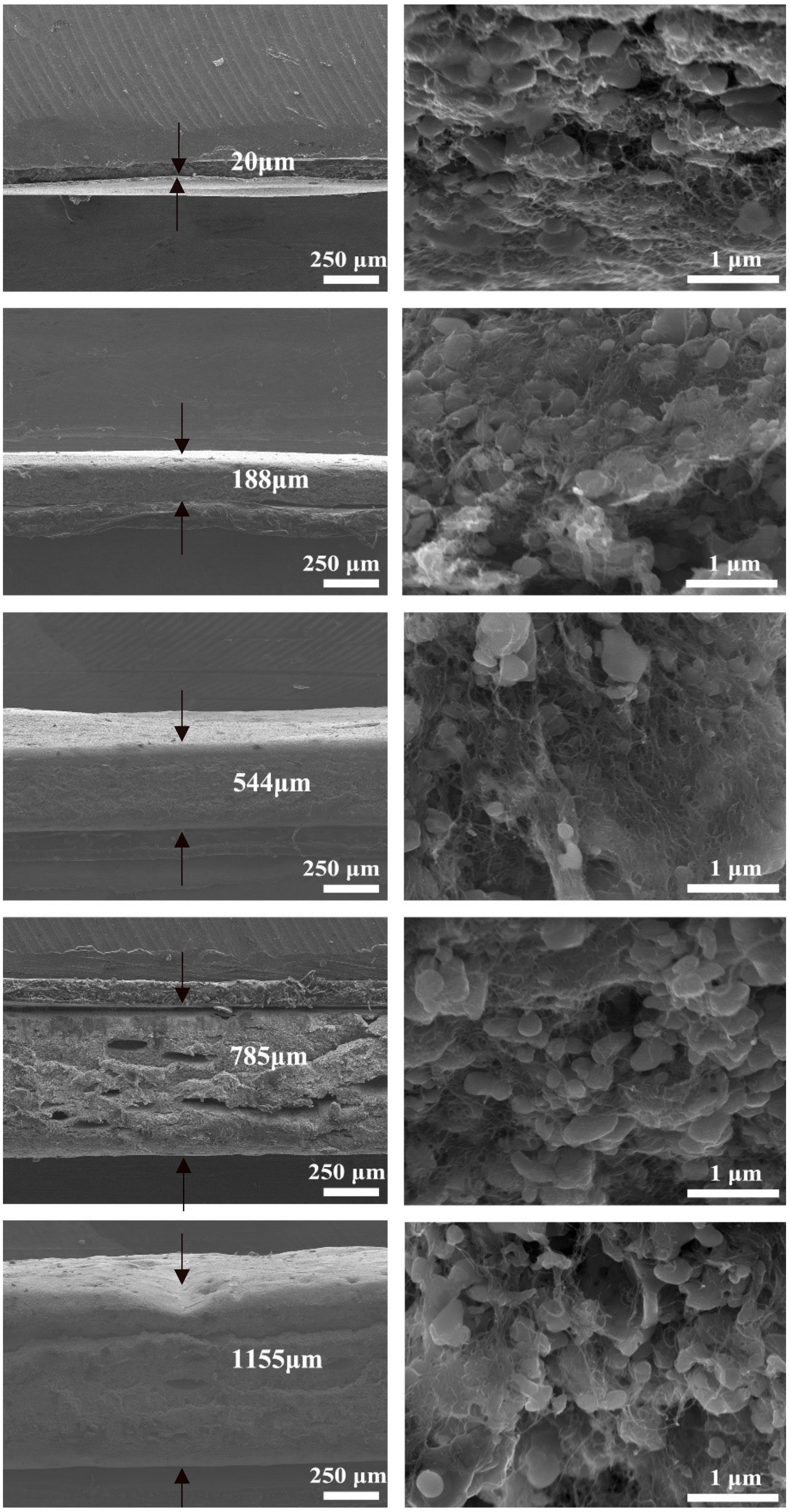

Fig S9. The cross-section images of LFP/CNT/TPAE electrodes with different thicknesses in the range of 20-1155 μm (left) and the corresponding microstructure of the cross-section (right).

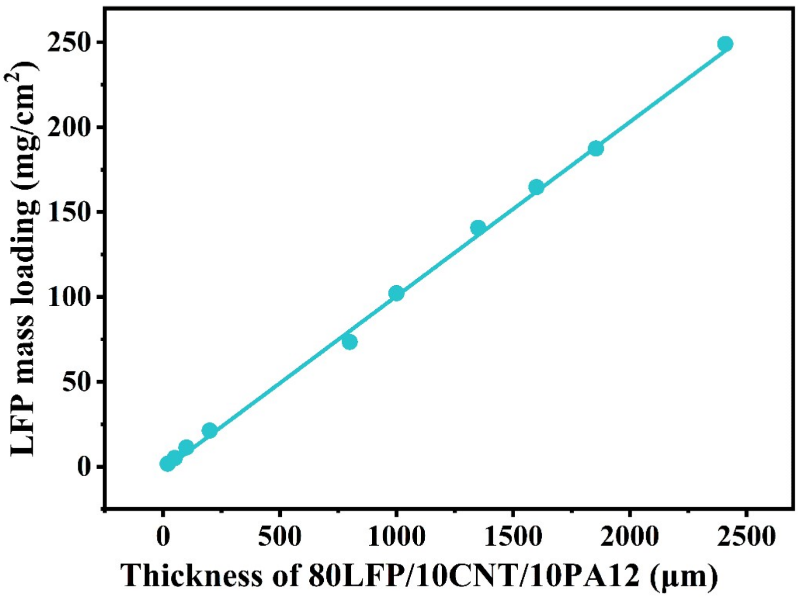

Fig S10. LFP mass loading in LFP/CNT/PA12 as a function of thickness.

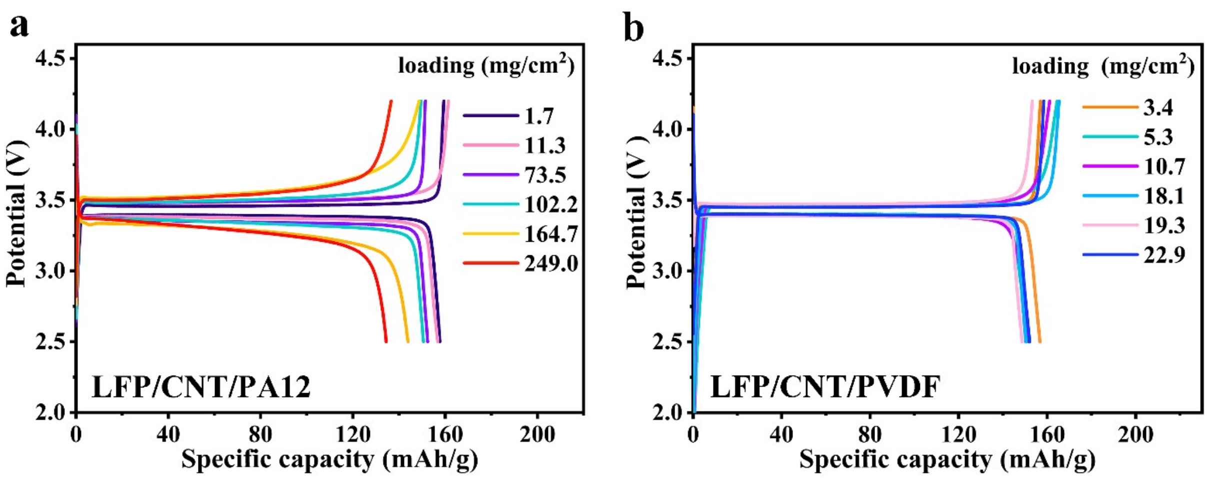

Fig S11. Charge/discharge profiles of (a) LFP/CNT/PA12 and (b) LFP/CNT/PVDF were collected at 0.1 C with different LFP mass loadings.

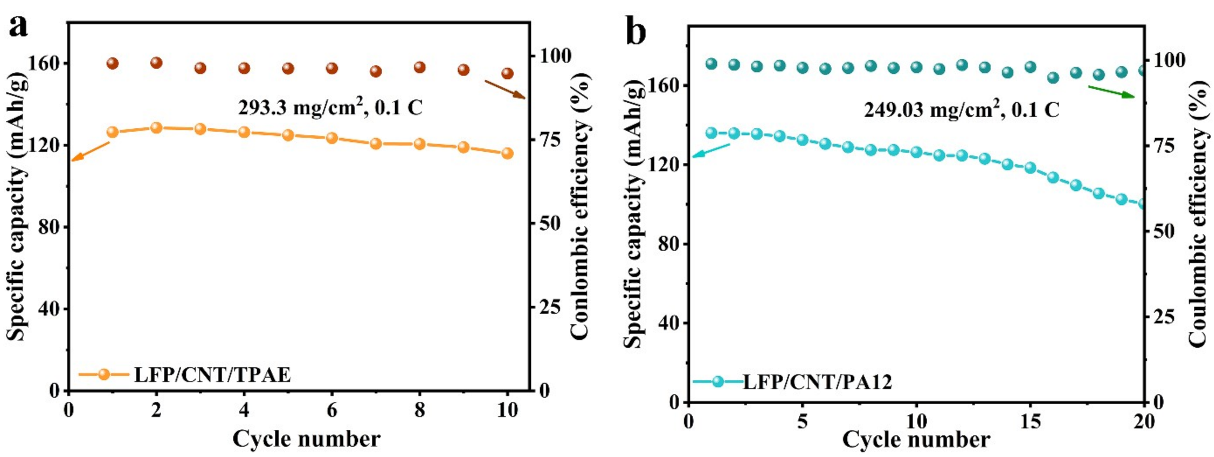

Fig S12. Cycling performance of (a) LFP/CNT/TPAE with the mass loading of 293.3 mg·cm^{-2} and (b) LFP/CNT/PA12 with the mass loading of 249.0 mg·cm^{-2} at 0.1 C.

Table S2. Areal capacity comparison of the water-based thick electrodes for LFP electrodes from literature and this work.

Electrode composition	Mass loadings ($mg \cdot cm^{-2}$)	Specific capacity ($mAh \cdot g^{-1}$)	Max. areal capacity ($mAh \cdot cm^{-2}$)	Ref
LMO/SuperC65/PL-CMC	20.3	113.0	2.3	[38]
NCM811/CNT/XG-KG	217.7	145.6	31.7	[39]
$LiCoO_2$/3C-binder	86.0	141.0	12.1	[40]
$LiMn_2O_4$/SWCNT	190.0	105.3	20.0	[41]
LMO/super-P/CMC-Li	70.0	100.0	7.0	[42]
LFP/CNT/TPAE	293.3	123.5	36.2	This work
LFP/CNT/PA12	249.0	136.0	33.9	This work

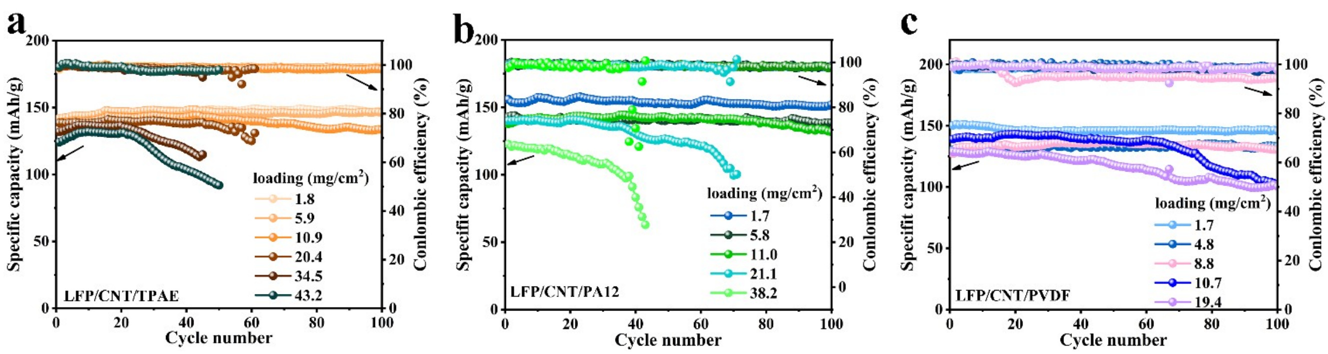

Fig S13. Cycling performance of (a) LFP/CNT/TPAE, (b) LFP/CNT/PA12, and (c) LFP/CNT/PVDF with different areal loading collected at 1.0 C.

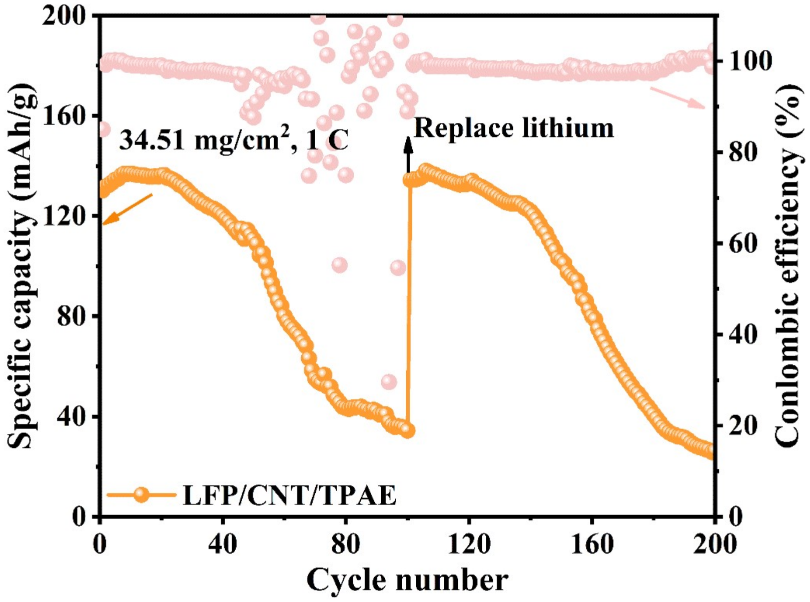

Fig S14. Cycle performance at 1.0 C of LFP/CNT/TPAE with a new Li metal anode at an LFP areal mass loading of 34.5 $mg \cdot cm^{-2}$.

Fig S15. Optical photographs of Li metal anode after 100 cycles of LFP/CNT/TPAE//Li cell with LFP areal mass loading of 34.5 mg·cm^{-2}.

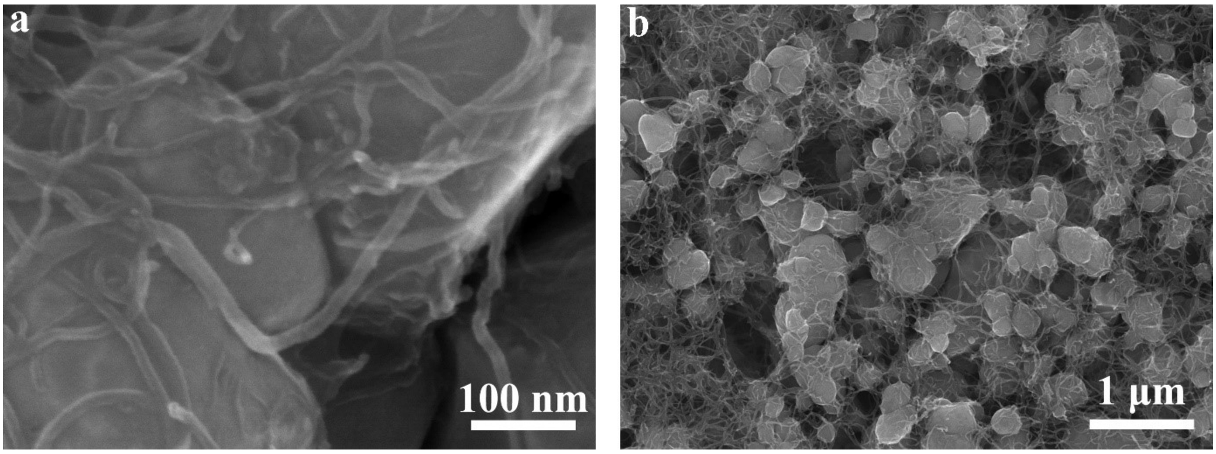

Fig S16. SEM images of 90LFP/5CNT/5TPAE.

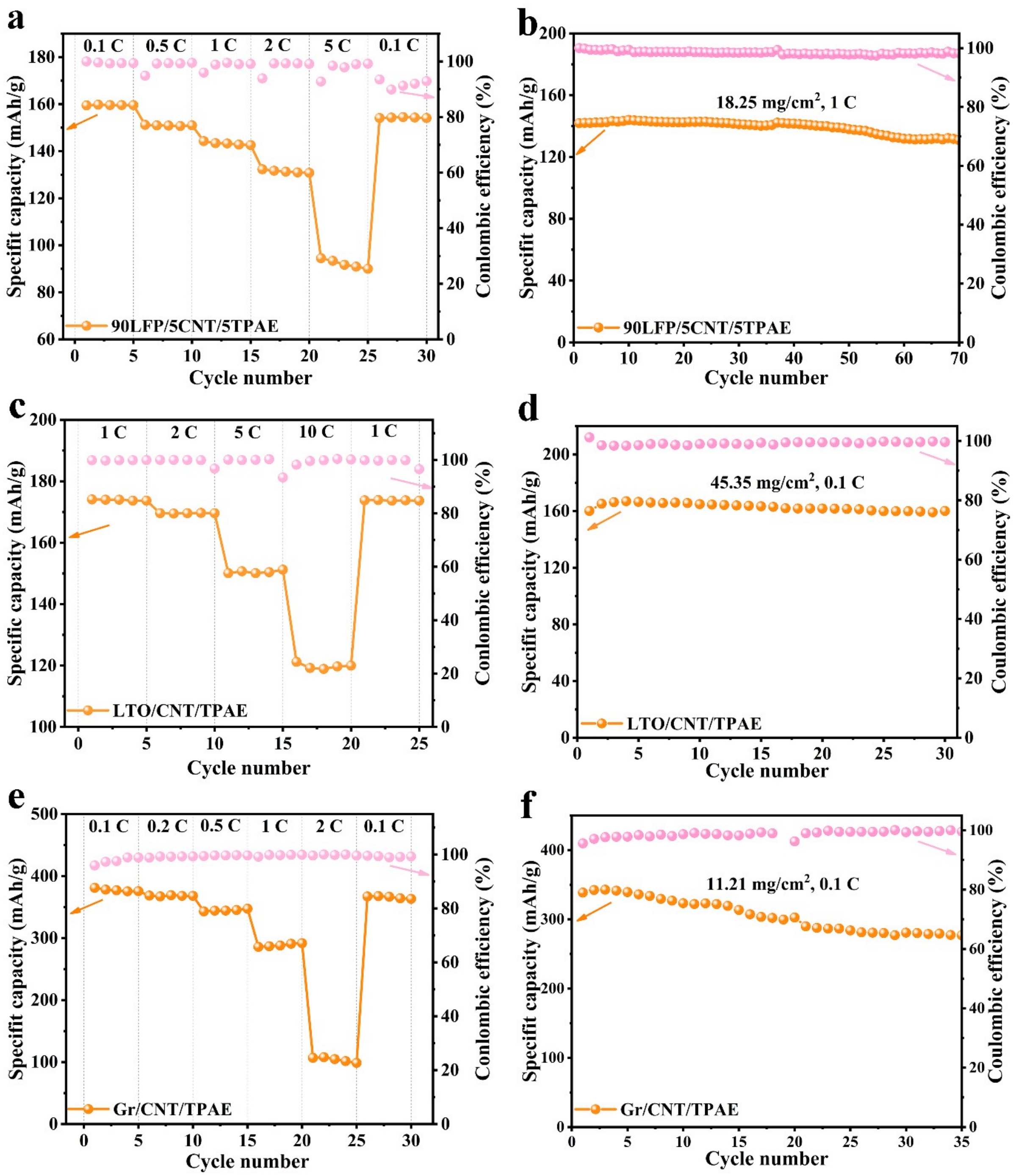

Fig S17. Rate capabilities of (a) 90LFP/5CNT/5TPAE with a mass loading of ~ 18.3 $mg\cdot cm^{-2}$, (c) LTO/CNT/TPAE with a mass loading of ~ 4.15 $mg\cdot cm^{-2}$, and (e) Gr/CNT/TPAE with a mass loading of ~ 2.29 $mg\cdot cm^{-2}$. Cycle performance of (b) 90LFP/5CNT/5TPAE, (d) LTO/CNT/TPAE, and (f) Gr/CNT/TPAE.

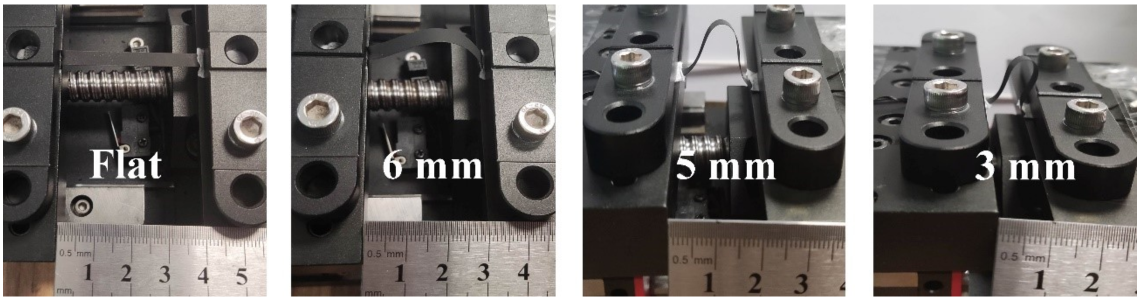

Fig S18. Corresponding digital photos of LFP/CNT/PA bending from a flat state to various bending radius of 6, 5, and 3 mm.

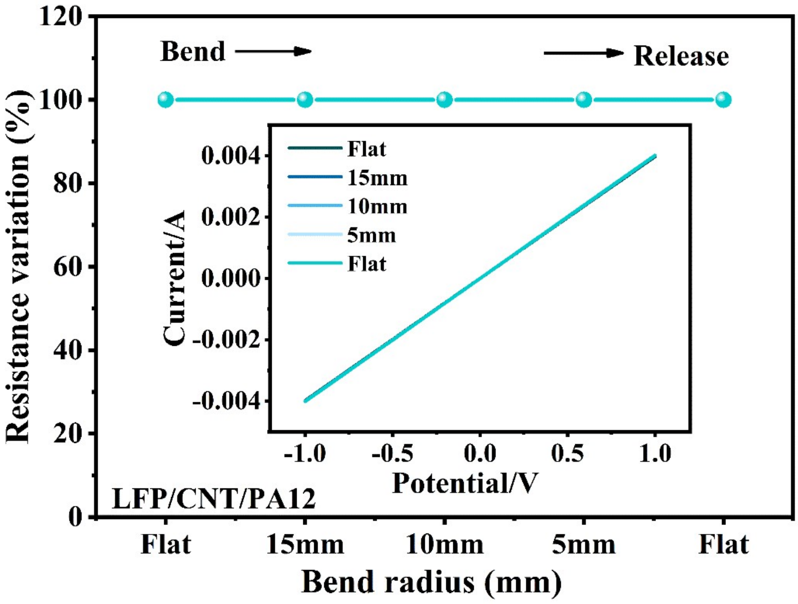

Fig S19. The LSV curves of LFP/CNT/PA12 when bent from a flat state to various bend radius and released to a flat state.

Equations:

Equation S1. The diffusion coefficients D of Li^+ were calculated according to the following equation:

$D_{Li} = R^2T^2/2A^2n^4F^4C_0^2\sigma^2$

Where D_{Li} is the Li^+ diffusion coefficient in LFP electrode ($cm^2 \cdot s^{-1}$), R is the gas constant (8.314 $J \cdot mol \cdot K^{-1}$), T is the absolute temperature (298 K), A is the surface area of the electrode (0.19625 cm^2), n is the number of electrons transferred per molecule during the electrochemical reaction (for LFP, $n = 1$), F is the Faraday constant (96485 $C \cdot mol^{-1}$), C_0 is the molar concentration of Li^+ in LFP (2.28×10^{-2} $mol \cdot cm^{-3}$), and σ is the Warburg factor associated with Z'.

Equation S2. Randles-Sevcik formule

$I_p = 2.69 \times 10^5 n^{3/2} A D_{Li}^{1/2} C_0 v^{1/2}$

where I_p is the peak current (A), n is the number of electrons transferred per molecule during the electrochemical reaction (for LFP, $n = 1$), A is the active surface area of the electrode (cm^2), C_0 is the molar concentration of Li^+ in LFP (2.28×10^{-2} $mol \cdot cm^{-3}$), D_{Li} is the Li^+ diffusion coefficient in LFP ($cm^2 \cdot s^{-1}$), and v is the scanning rate ($V \cdot s^{-1}$). According to this formula, D_{Li} is proportional to $I_p^{-1/2}$.